

Multi-scale Characterization of Lithium Ion Battery Cathode Material by Correlative X-ray and FIB-SEM Microscopy



Multi-scale Characterization of Lithium Ion Battery Cathode Material by Correlative X-ray and FIB-SEM Microscopy

Authors: Christian Weisenberger, Andreas Kopp,
Timo Bernthaler, Volker Knoblauch,
Gerhard Schneider
*Institut für Materialforschung,
Hochschule Aalen, Germany*

Heiko Stegmann, Holger Blank,
Alexander Orchowski, Fabián Pérez-Willard
Carl Zeiss Microscopy GmbH, Germany

Date: June 2015

In this Application Note, a multi-scale study of the LiMn_2O_4 cathode material of a commercial 18650 lithium ion battery is presented. X-ray microscopy (XRM) measurements of the cathode reveal unexpected features which motivate more detailed analysis in the FIB-SEM. These features of interest are sparse and located at random locations well below the sample surface. In a correlative approach, the XRM data set is used as a reference to make site-specific FIB cross sectioning and tomography possible.

Introduction

Lithium-ion batteries (LIB) are wide spread as rechargeable power sources for portable electronics devices. As compared to other battery chemistries LIBs feature high energy densities, no memory effect and a relatively low self-discharge when not in use [1, 2]. These advantages explain their rapid spread in the market ever since their commercial introduction in 1991 [3]. Other growing applications for LIBs are electric mobility and stationary energy storage. Overall, the market for lithium ion batteries is developing extremely fast and is expected to reach a \$25 billion volume by 2017 [4].

The main components of the LIB are anode, cathode, separator and electrolyte. Very often the cathode material is a lithium transition metal oxide (e.g. LiMn_2O_4 , or $\text{LiNi}_x\text{Co}_y\text{Mn}_z\text{O}_2$). It is the source of lithium ions. For the anode, graphite is often used as active material. During charging, the cathode is delithiated, i.e. lithium ions move from the cathode through the separator to the anode, where they are intercalated into the carbon layers of the graphite. Each ion stores a certain amount of energy which is retrieved during battery operation (discharge).

Life time and performance of the LIB are mainly determined by the constituent active materials and the microstructure of the active mass coating. Important parameters are particle size, shape and distribution, the presence of voids and defects within the particles, porosity, pore tortuosity, and coating thicknesses. In many cases, two-dimensional microscopy studies from mechanically prepared cross sections are not sufficient for the full characterization of the LIB electrodes. This calls for a three-dimensional (3D) multi-scale microscopy approach.

In this Application Note, a post-mortem study of the cathode material of a commercial LIB is presented. X-ray microscopy (XRM) measurements reveal the microscopic structure of the cathode active material non-destructively. Additionally, a few unexpected strong X-ray scattering centers are detected. These motivate high-resolution FIB-SEM work to determine their origin. A powerful new correlative method is presented that enables XRM supported site-specific FIB-SEM navigation.

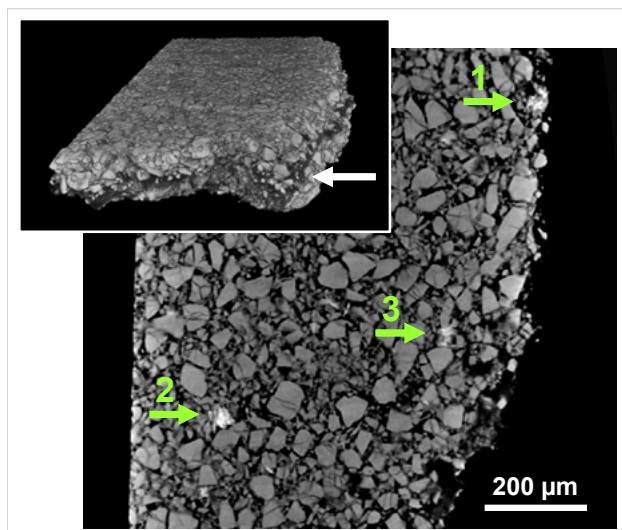


Figure 1 Top left: 3D volume reconstruction of an XRM data set from the cathode sample. Bottom right: virtual cross section through the XRM volume showing three bright spots (green arrows) of unknown origin.

Materials and Methods

For the following study a commercial cylindrical battery, type 18650, was used. According to the material safety data sheet for this battery, the cathode material is LiMn_2O_4 and the anode material is graphite. The cell was discharged and cut open in a glove box under protective Ar atmosphere. Cathode, separator foil and anode were carefully separated. A small piece of the cathode was cut using a scalpel. The resulting sample is needle shaped with dimensions of approximately $L \times W \times H = 6 \text{ mm} \times 800 \text{ }\mu\text{m} \times 200 \text{ }\mu\text{m}$. The sample was glued to the end of a steel needle support. Thus, the sample is free standing for the XRM analysis.

XRM measurements were performed on a ZEISS Xradia 520 Versa system. Similar to a computed tomography system (CT) the sample is illuminated with X-ray Bremsstrahlung coming from a high-brightness laboratory X-ray source. Projections of the sample are recorded in a unique two-stage magnification process which includes optical magnification. For rendering and visualization of the XRM data sets the software Visual SI from ORS was used.

High resolution 3D as well as EDS analysis of specific sites of the sample was carried out using a FIB-SEM instrument ZEISS Crossbeam 540. Targeted navigation to these sites of interest was enabled by the correlative ZEISS Atlas 5 software package on the FIB-SEM.

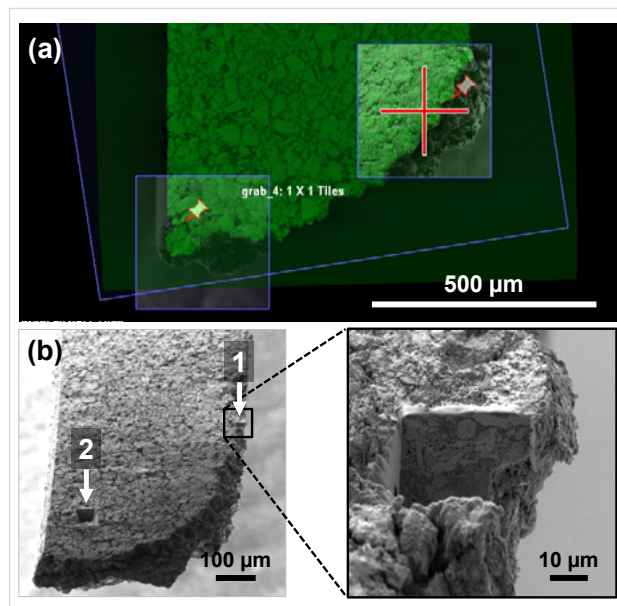


Figure 2 (a) Overlay of SEM (grey) and XRM (green) images. After successful correlation, the XRM data is used as a reference for FIB-SEM navigation. (b) SEM overview image of the sample. Sites of interest are highlighted by the white arrows. The inset shows a detail of Site 1.

XRM Results & Correlative Navigation

The inset in Figure 1 shows an overview image of a 3D rendered XRM data set from the cathode sample. The white arrow indicates a roughly $20 \text{ }\mu\text{m}$ -thick aluminum foil sandwiched between two layers of LiMn_2O_4 . This aluminum foil serves as a substrate for the active material coating during cathode production and as current collector.

The main image in Figure 1 shows an arbitrary virtual section through the XRM volume. This section is contained within the upper LiMn_2O_4 layer (cf. inset). The morphology of the LiMn_2O_4 particles (i.e. size, shape) is revealed clearly. Even cracks inside the active material particles can be resolved. Furthermore, three bright spots – highlighted by the green arrows – are visible in the image, too. Such strong X-ray scatterers are sparse in the sample. They are all located below the surface. Their origin and composition are unknown and were elucidated by FIB-SEM analysis.

The challenge was to access the aforementioned sub-surface sites of interest in the FIB-SEM instrument. For this purpose the XRM data set was imported and displayed in the FIB-SEM user interface (UI) of Atlas 5. The XRM data set was oriented and sectioned by the user aiming to obtain a 2D image

which resembles the SEM view in the FIB-SEM instrument. Figure 2(a) shows an overlay of SEM (grey) and XRM (green) images. Distinctive features of the sample surface visible in both SEM and XRM image are lined up and used to lock the XRM reference image to the SEM stage coordinate system. With this is accomplished, targeted, even automated FIB-SEM work of the sub-surface sites of interest becomes possible.

Two sites of interests, Site 1 and Site 2, were studied in more detail by FIB-SEM. The white arrows in Figure 2(b) mark these two sites. The inset shows a detail of the FIB cross section through Site 1.

FIB-SEM Results & Discussion

Figure 3 shows SEM images of the cross section at Site 1. (a) is an SE image obtained at 2 kV SEM acceleration voltage with the chamber SE detector. Particles of different sizes and shapes are revealed. The gaps between the particles are not fully filled by binder material. (b) was acquired simultaneously to (a) with the backscattered electron InLens EsB detector. The backscattered signal contains information about composition. In the EsB image, the binder material – of organic nature – appears very dark. The particles appear in two brighter, but significantly different, levels of grey. This is a first hint that particles of two different compositions are present in the region of interest. This finding is confirmed by EDS measurements. The EDS map in image (c) shows the distribution of manganese (red) and lanthanum (green) in the cross section. The particles with the brightest contrast in the EsB image are rich in lanthanum and contain no manganese.

A second cross section of Site 2 yields exactly the same results, which leads to the conclusion that all anomalies observed in the XRM data correspond to agglomerates of lanthanum rich particles.

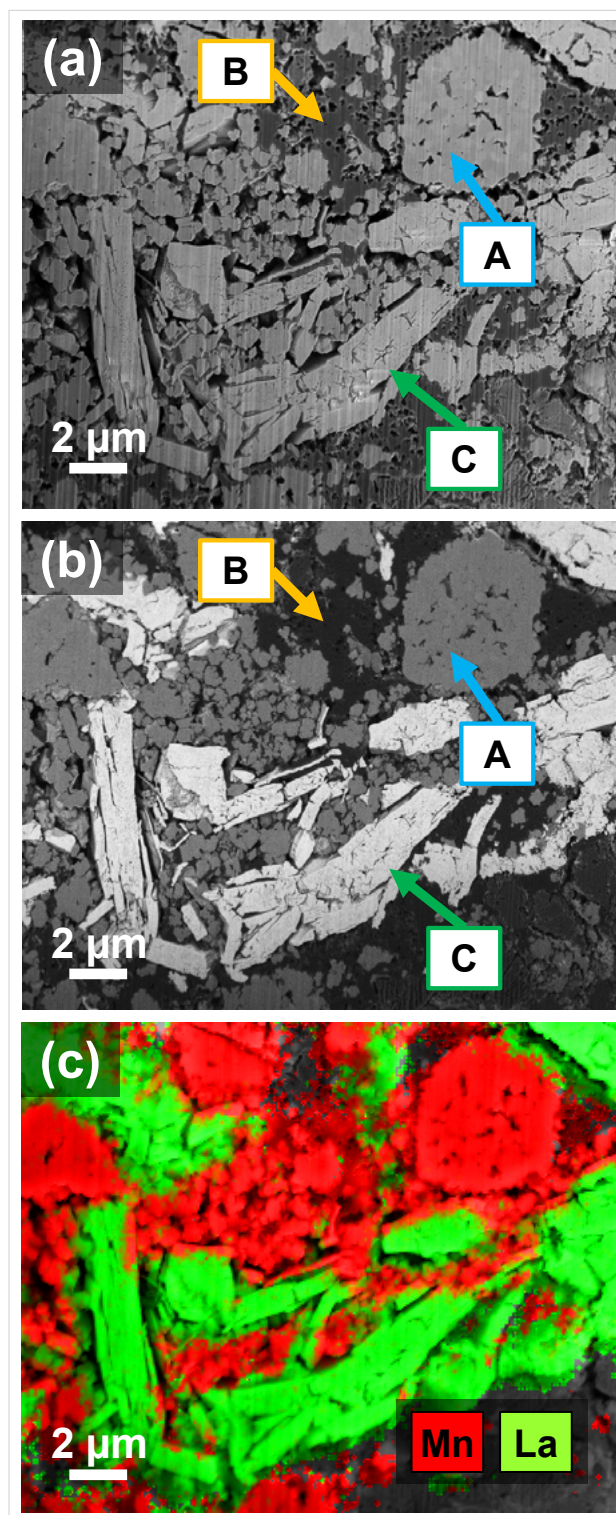


Figure 3 SEM images of a cross section of Site 1. The SE (a) and EsB (b) images were acquired simultaneously (A = LiMn_2O_4 , B = binder/conductive agent, C = lanthanum particle). (c) shows an EDS map of the cross section showing the distribution of lanthanum (red) and manganese (green).

Interestingly, a second small agglomerate, which was not apparent on first sight in the XRM data, was discovered near the surface in the EsB cross section image of Site 2 (see left of Fig. 4). It shows the same contrast as the larger agglomerate detected by XRM. EDS spectra from both inclusions are indeed identical (see right hand of Fig. 4). We conclude that the cathode material contains far more lanthanum-rich agglomerates or particles than originally assumed after our first analysis of the XRM data. Equipped with this knowledge a more accurate study of the XRM data becomes possible.

At the time of writing, the reason why the lanthanum-containing particles are present in the cathode material of this LIB remains uncertain. Lanthanum can be used as a dopant for cathode active materials [5]. However, in these cases lanthanum is only added in small quantities [6, 7]. Moreover, Lithium-lanthanum-titanium-oxides (LLTO, $\text{Li}_{3x}\text{La}_{2/3-x}\text{TiO}_3$) are known to be used as ionic conductors (solid electrolyte) in lithium-ion batteries [8]. Such particles could have been used as additives to the active mass. However, because the EDS spectra do not show any titanium peaks, we can rule out this possibility.

Summary

In this study, it is shown that with XRM a very powerful technique for the non-destructive 3D characterization of the active mass coatings of LIBs is at our disposal. When combined with FIB-SEM microscopy, unprecedented high-resolution multi-scale studies become possible. ZEISS Atlas 5 provides an efficient correlative workflow platform to easily perform XRM-assisted FIB-SEM examinations of targeted sub-surface features in the sample.

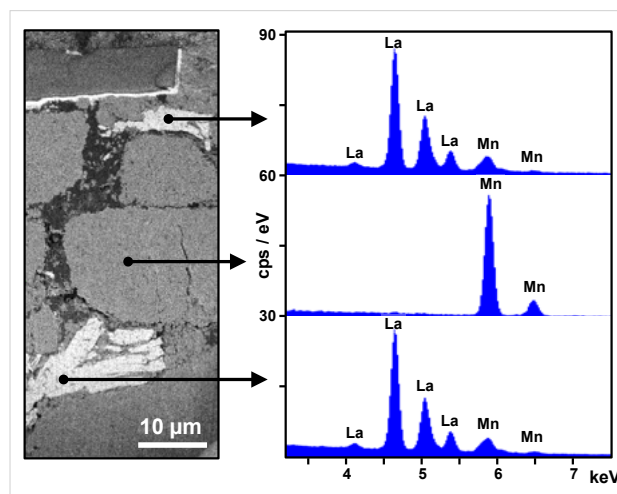


Figure 4 EDS measurements from a cross section of the sample at Site 2. The spectra were acquired in spot mode from the locations marked by the arrows in the EsB image. For clarity, in the diagram the spectra are shifted upward consecutively by 30 cps/eV from bottom to top.

References:

- [1] For a recent review, Lithium-Ion Batteries: Advances and Applications, Ed. G. Pistoia, Elsevier (2014).
- [2] Lithium Ion Rechargeable Batteries: Materials, Technology, and New Applications, Ed. O. Kazunori, Wiley-VHC (2009).
- [3] T. Nagura, Prog. Batteries & Battery Materials 10, (1991), 218.
- [4] Global Market for Lithium-Ion Batteries - Forecast, Trends & Opportunities 2013–2020, http://www.researchandmarkets.com/reports/2599948/global_market_for_lithiumion_batteries (2013).
- [5] J. W. Fergus, Recent developments in cathode materials for lithium ion batteries, Journal of Power Sources 195 (2010), 939–954.
- [6] A. Iqbal et al., Enhanced electrochemical performance of La- and Zn-co-doped LiMn_2O_4 spinel as the cathode material for lithium-ion batteries, J. Nanopart. Res. 14 (2012), 1–14.
- [7] P. Ghosh et al., Lanthanum-doped LiCoO_2 cathode with high rate capability, Electrochimica Acta 54 (2009), 1654–1661.
- [8] P. Knauth, Inorganic solid Li ion conductors: An overview, Solid State Ionics 180 (2009), 911–916.



Carl Zeiss Microscopy GmbH
07745 Jena, Germany
microscopy@zeiss.com
www.zeiss.com/microscopy



We make it visible.